Novel Bidirectional Elastic Nonlinear Element (BENE) for Robotic Antagonistic Actuation

by

Juan-Diego Florez-Castillo

A Thesis

Submitted to the Faculty of the

WORCESTER POLYTECHNIC INSTITUTE

In partial fulfillment of the requirements for the

Degree of Masters of Science

in

Robotics Engineering

by

_____

August 2020

APPROVED:

_____
Dr. Marko Popovic, Advisor

_____
Dr. Gregory Fischer, Committee Member

_____
Dr. Michael Gennert, Committee Member

Abstract

To expand extra-planetary mission support capabilities, highly specialized robotic systems are developed and implemented that are not generalized enough for successful implementation across multiple environments. Here, a tetrapodal robot capable of task-oriented locomotion and manipulation is envisioned that can serve as a robust platform for mission support across multiple gravitational environments. The proposed system, referred to as the Trans-Gravitational Robot (TGR), is anticipated to operate in orbital, Lunar, and Martian environments by employing dexterous limbs capable of compliant actuation for both locomotion and manipulation.

A simplified robot limb design with variable stiffness and compliance is proposed as a proof of concept of essential technologies for the development of the TGR. Antagonistic actuation is achieved using a novel, nonlinear, torsional spring module, coined the Bidirectional Elastic Nonlinear Element (BENE). A design approach for this elastic element was produced, which allows for scalable and customizable elastic element designs to be produced using the same basic approach. The implementation of the BENE modules for antagonistic actuation enabled the decoupled and straightforward control of position and stiffness. The BENE and its accompanying control scheme were developed and validated as proof-of-concept for variable stiffness actuation for the TGR limb.

Acknowledgements

I would like to first thank my advisor Dr. Marko Popovic of Worcester Polytechnic Institute (WPI) for his support throughout the duration of this thesis and my education at WPI. He pushed me to be a better researcher and provided valuable advice and criticism that shaped my development and the development of this project. My experience working with him provided invaluable insight for my research career moving forward.

I would also like to thank Professor Gregory Fischer and Professor Gennert for taking the time to review my thesis. Professor Fischer shaped my experience as a teaching assistant and helped me develop skills that will make me a better educator and researcher. He provided me with career advice and I am very grateful to him. I am thankful to Professor Gennert for imparting not only advice, but also technical knowledge, which helped me grow not only as a researcher but also as a roboticist. He is an excellent professor, and I am thankful to have been able to learn from him.

I would like to thank Felix Sanchez of WPI for collaborating with me on the Trans-Gravitational Robot project, which inspired this thesis. He has been a valuable friend and fellow Popovic Labs member during this project, and his insight and input has served to improve the quality of this work.

Finally, I would like to thank my parents, my sister, my brother, and my future wife, Mariana Velazquez, for their unwavering love and support throughout the years. They made this accomplishment possible and inspire me to continue growing as a researcher and as a person.

- Juan-Diego Florez-Castillo

Contents

List of Figures

List of Tables

Chapter 1

Introduction

1.1 Background and Motivation

The ongoing and increasing commercialization of space travel has renewed interest in the exploration and colonization of space and non-terrestrial environments. These environments present unique challenges through volatile and potentially hazardous conditions for humans, a problem that has historically been addressed by highly specialized systems designed to operate in the conditions present in those environments. For instance, the carefully designed and constructed Mars rovers, with their assortment of instruments, have been engineered for missions specific to the Martian surface, which is regularly subjected to hazards including large doses of radiation, dust storms, and a wide range of temperatures [1] [2]. Replacing humans as the physical movers in such missions greatly reduces risk and could even expand mission potential. Human-robot interaction and human-in-the-loop robotic systems can address many potential hazards and simplify difficult tasks in multiple non-terrestrial environments. Tasks involving exploration, maintenance, and experimentation could be automated or simplified by having a robot carry out the physical

labor while a human addresses the higher-level decision-making. For example, the Curiosity rover currently employs advanced autonomous path-planning combined with human command inputs for navigation [3], similar to the human-in-the-loop, heuristic path planning algorithm described in [4]. While this is an example of a human-involved system, strides are being made to expand this to a much more developed "shared control" paradigm wherein the human-robot system benefits from a more robust and adaptable control approach [5]. To address the need for a robotic platform that can expand the scope and potential of mission support tasks while supporting advanced control approaches, the Trans-Gravitational Robot (TGR) is proposed. The TGR is envisioned to be capable of task-oriented locomotion and manipulation in various gravitational environments including orbital, Lunar, and Martian conditions.

1.1.1 Locomotion

Because mission environments can differ significantly, robotic systems have historically been designed to carry out limited, specific tasks with specialized hardware. For robots capable of task-oriented locomotion, the locomotion method is carefully considered and developed to be best suited for the specified mission environment. Various locomotion methods have been developed for robots operating in non-terrestrial environments. A well known example, the Mars rovers, one of which is shown in Fig. 1.1, use wheeled locomotion in the form of the rocker-bogie assembly to traverse the Martian environment [3]. Wheeled locomotion is useful under gravitational loading conditions, as it can provide a more energy efficient means of locomotion on a variety of terrains. However, wheeled locomotion is limited by terrain conditions, as it requires a continuous floor plane, and uneven terrain can present obstacles that must be traversed slowly or circumvented entirely. As a result, wheeled robots require

careful path planning in order to avoid hazardous terrain in order to mitigate their limited capacity to traverse it. Moreover, the Mars Helicopter, Ingenuity, which will work in parallel with the Mars 2020 rover, Perseverance, will use propellers for aerial surveying on the Mars 2020 mission [6]. This locomotion method requires an atmosphere or fluid medium and suffers from lack of efficiency from a long-term mission scope.

Figure 1.1: The Perseverance Mars Rover (Mars 2020) [3](left) and the Ingenuity Mars Helicopter (right) [6]

Similarly, the Astrobee robots, shown in Fig. 1.2, use propulsion to traverse micro-gravity environments in orbital gravitational conditions on the International Space Station (ISS). They are equipped with propellers and exhaust nozzles for compressed gas, which serve for controlled translation and rotation in micro-gravity [7]. However, while this method is effective in enclosed micro-gravity environments, such as within the ISS, it is not suited for other gravitational conditions. In comparison, limbed locomotion has proven to be more robust for difficult terrain and is viable within enclosed micro-gravity environments, as exemplified by astronaut locomotion in the ISS. Understanding the utility of limbs in micro-gravity, a manipulation limb is being developed for the Astrobee to help the it stabilize trajectories without needing to use propulsion [8], thus allowing it to serve as an example for the viability of limbed locomotion for robots in micro-gravity.
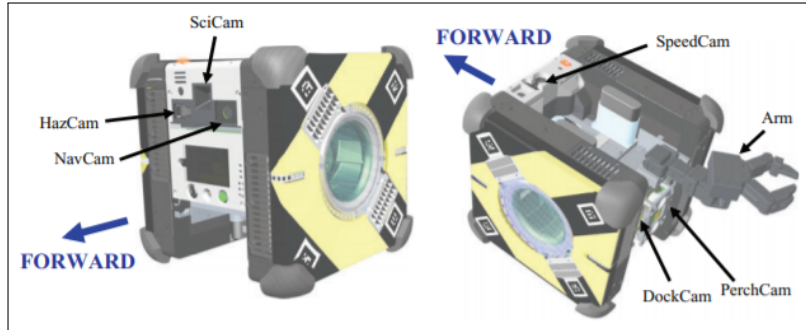
Figure 1.2: The Astrobee robot's body layout [8]

Unlike with the previously described locomotion methods, limbed locomotion in humans has been shown to work across different gravitational environments, as evidenced by successful missions in orbital and lunar conditions. Thus, unlike most modern space robots capable of locomotion, humans can perform task-oriented locomotion and dexterous manipulation in multiple gravitational environments. Ongoing research into space humanoid robotics with the Robonaut 2 (R2), NASA's most advanced humanoid robot, is meant to support and replace astronauts in specific tasks [9]. R2, shown in Fig. 1.3, is equipped with 2 dexterous manipulators and is intended to serve as a research platform for potential dexterous mission support [9]. However, the end effectors currently used on its lower limbs are not intended for body-weight support [9], as they are primarily used to affix R2 to the handles located throughout the ISS, thus making it a four-armed robot. To expand on the functionality of this form factor, the TGR should be a tetrapod, with each limb being capable of operating as a both a manipulator (arm) and as a locomotion limb (leg).

Such a body structure would allow the TGR to approximate the dexterity and robustness of humans in their task environments. For instance, on Lunar and Martian environments, the robot could walk, bound, and climb if necessary. Similarly, in environments similar to that found in the ISS, the TGR could push against fixed

Figure 1.3: Robonaut 2 showing its manipulation limbs and locomotion limbs, the latter of which are see anchoring it to the hand rails of the ISS [23].

surfaces and interact with handles in much the same way astronauts do. Because each limb could act as a manipulator, the TGR is anticipated to dexterously manipulate objects of interest. The aforementioned functionality requires the development of a robust limb with an estimated 6 degrees of freedom (DOF).

1.1.2 Actuation

For a limbed robot to operate safely within close proximity to humans (in the shared space of the ISS), a high level of compliance control is necessary. There are two main types of compliance that could be implemented to a system: passive compliance and active compliance. Passive compliance involves the implementation of a mechanically compliant actuation method, typically through the implementation of an elastic element. In contrast, active compliance uses control approaches to approximate a passive compliant response [10]. While it can approximate passive compliance, ac-

tive joint compliance cannot fully mimic the performance of a passively compliant system, and this would require an ideal, error free system with an infinitesimally brief feedback loop. Thus, a passive compliance method using elastic elements in the joints was implemented. This implementation was akin to the implementation of a series elastic actuator, or SEA, and allowed for the following benefits [11] [12]:

- It reduces impacts and disturbances on the actuators and joints, thus increasing the robustness of the system and its ability to react to disturbances.

- It is capable of storing and releasing energy as necessary to improve efficiency.

- It provides passively compliant actuation for safer operation in a human-shared environment.

- It can be used for admittance control based on the elastic element's positional information.

While there are four main stiffness control methods as described in [12], the most bio-mimetic is antagonistic controlled stiffness. This approach mimics the decoupled joint position and stiffness achievable by antagonistic muscle pairs, which are recruited as needed within the control loop. For a robotics application, this is achievable with two actuators and nonlinear springs between the actuators and the load, as shown in Fig. 1.4 [12]. Variable stiffness actuation (VSA), which is achievable through antagonistic actuation, requires nonlinear elastic elements in order to successfully vary the equivalent stiffness of the system. Linear springs have a constant stiffness value, which, while effective in other compliant systems, would be ineffective for VSA because the stiffness is constant for all loading of the elastic element. With nonlinear springs, the two motors can, together, control both DOF of an antagonistically actuated joint, position and stiffness. This is possible because

the equilibrium position between the springs and the preload between them affects the position resulting equivalent stiffness of the actuated joint.
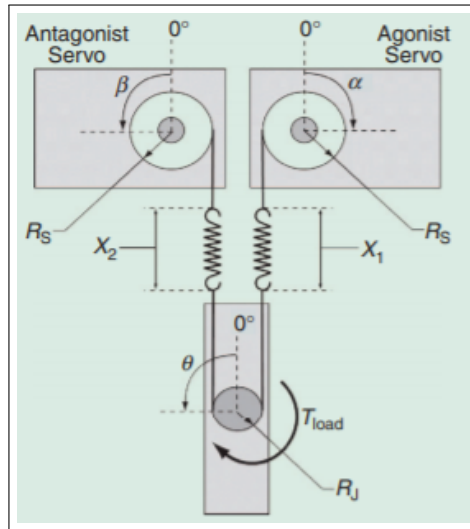
Figure 1.4: Basic diagram describing an antagonistic actuation approach [12]

To this end, a low-cost, scale-able, nonlinear element was developed, known as the Bidirectional Elastic Nonlinear Element (BENE). The BENE module acts as a nonlinear spring and enables variable stiffness actuation and passive compliance in the rotary joints of the envisioned TGR robot.

1.2   Problem Statement

The development of a robust robotic platform capable of expanding the mission support capabilities of previous space robots is the end goal of the overarching TGR project. For the robot to operate effectively in enclosed orbital environments, such as the ISS, as well as on the Lunar surface, the robot must be designed to be lightweight, dexterous, safe to operate in human-shared environments, and capable of limbed locomotion.

This thesis will focus on the development of a simplified TGR limb, capable

of being expanded on to achieve full task-oriented locomotion and manipulation, as well as the development and verification of the BENE-module antagonistic actuation approach. The TGR limb, with the aforementioned actuation approach, will be able to vary stiffness and position as necessary in its join trajectories. This capability will allow the TGR to benefit from disturbance reduction, shock absorption, energy storage, and admittance control from the implementation of the BENE module alone.

1.3   Scope

The main objectives are as follows:

1. Design a simplified limb for the TGR with capabilities for mobility and manipulation.

2. Develop the Bidirectional Elastic Nonlinear Element (BENE) for compliant actuation and variable stiffness. The method used to develop the BENE should be intuitive and user customizable. The method used should reject invalid configurations and show a simulated stiffness profile of valid configurations.

3. Demonstrate the capabilities of the BENE module in antagonistic actuation and validate its use as an elastic element for variable stiffness systems used for locomotion and manipulation.

Chapter 2

Related Work

2.1 Robots with Versatile Limbs

Limb design of limbed robots is integral to their functionality, as affects the efficacy of their locomotive limbs (if they are equipped with them) as well as their manipulators. Limb versatility involves designing the limbs such that they can be used to accomplish multiple operative tasks such as manipulation and enabling mobility. For example, NASA JPL's ATHLETE Rover, shown in Fig. 2.1, is equipped with limbs with wheels at their ends, the actuators of which can be used to drive a tool end effector unique to each limb [13]. The ATHLETE can benefit from the efficiency of wheeled locomotion on even terrain, and also use its limbs to interact with its environment or navigate obstacles, increasing the versatility of the robot as a whole in terrestrial environments.

This limb design approach was updated for the smaller RoboSimian, which also used wheels at the end of each of its limbs. However, unlike the ATHLETE rover, the RoboSimian was designed with actuated wheels mounted on one of the elbow joints on its limbs rather than as part of the end effector [14]. This change allowed the

Figure 2.1: The ATHLETE Rover on uneven terrain [13]

RoboSimian to be equipped with swappable foot and gripper end effectors, which would need to be changed by an operator as necessary. However, a gripper able to be used as a foot was also created [14]. The RoboSimian and its versatile end effector are shown in Fig. 2.2.

Figure 2.2: RoboSimian traversing uneven terrain at the 2015 DARPA Robotics Challenge (left). The versatile gripper (Right) had under-actuated digits and a palm designed to support the weight of the robot [14]

Another robot that uses its limbs for both mobility and manipulation is the Robonaut 2 (R2). R2 is equipped with two manipulator limbs, referred to as its arms, and 2 dedicated anchoring limbs, referred to as its legs. R2, shown in Fig. 1.3, is equipped with series elastic actuators in each 7 DOF limb [15]. While it does

have dedicated arms and legs, R2 uses gripping as its means of mobility, pushing and pulling itself along the handrails located throughout the ISS as seen in Fig. 2.3. In other words, R2 displays versatile limbs that would be used in the same way a primate with prehensile feet might use its limbs in micro-gravity.

Figure 2.3: Without using its arms, R2 can navigate the ISS by anchoring onto the handrails (right) [24].

Robosimian and R2 inspired the design of the TGR limb, as they are both capable of using their end effectors for manipulation and mobility. RoboSimian's specialized gripper is an example of a potential envisioned end effector for the TGR. Moreover, R2's ability to interact with tools and equipment while anchoring itself to the handrails is a desired end goal for the TGR; however this capability is sought for each of its limbs so that none of its limbs can be specified as being for locomotion only.

2.2 Variable Stiffness and Antagonism

Variable stiffness actuation allows robots to directly and independently control the position and stiffness of their joints. Series-elastic-based variable stiffness actuators (VSAs) typically operate through one of four approaches: equilibrium controlled stiffness, antagonistic controlled stiffness, structure controlled stiffness, or mechanically controlled stiffness, as described in [12]. In these systems, elastic elements are placed between the actuator(s) and the load in configurations that would allow the equivalent spring stiffness (k) of the system to be varied. Specifically, in an antagonistic system, two non-linear springs are attached in parallel to a load, each with its own motor, as shown in Fig. 1.4. By varying the equilibrium position between the springs as well as the preload of them, the equivalent stiffness and position of the joint can be controlled.

Antagonistic actuation operates using the same principle as antagonist muscle pairs, such as the biceps and triceps, which can be tensed to varying degrees to increase or decrease the stiffness of a joint as well as change its angular position. However, muscle recruitment also affects the resulting joint stiffness, as the recruitment of individual motor units is what affects the degree to which a muscle will pull at a joint [16]. This approach has been applied to fluid-based artificial muscles such as the Mckibben Muscle [17] [18] and the HydroMuscle [19] [20], allowing for the controlled stiffness and position of a joint. In Fig. 2.4, a muscle recruitment diagram of a Mckibben muscle configuration can be seen.

The use of a bidirectional elastic element allows the joint to benefit from the ability of motors to pull in both directions, which muscles are incapable of [21]. Bidirectional elements are typically pairs of "directional" springs, such as tensile springs, arranged as in Fig. 2.5.
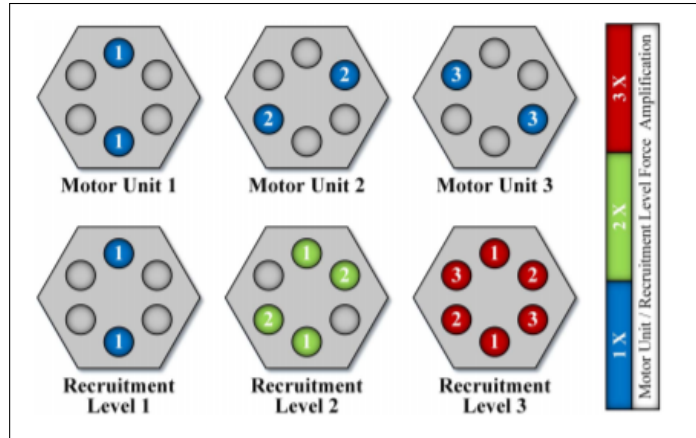
Figure 2.4: Basic diagram describing muscle recruitment, in which pairs of opposing Mckibben Muscles are activated to increase the power of the muscle group [18]
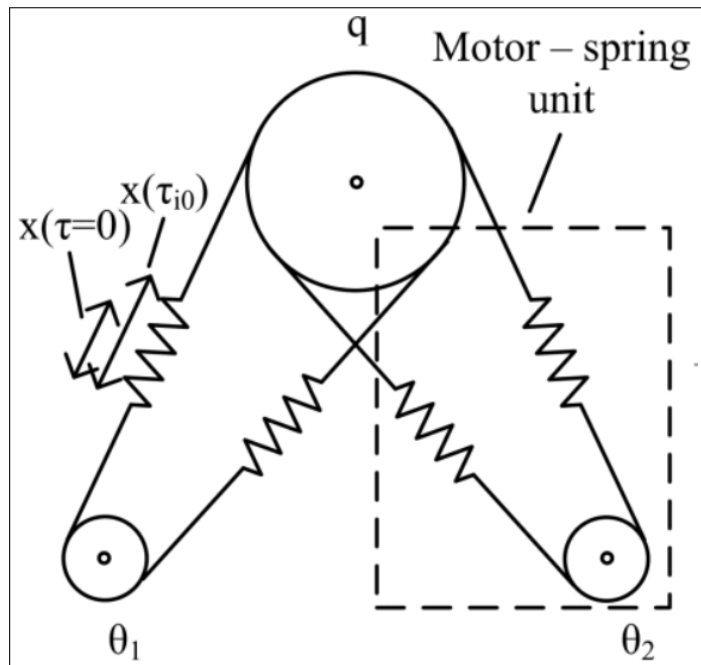
Figure 2.5: Basic diagram describing a bidirectional, antagonistic actuation approach [21]

Chapter 3

Methodology

The variables used in the design and development of the system can be found in table 3.1:

3.1 Trans-Gravitational Robot Limb

3.1.1 Design Considerations

The TGR's intended use for task oriented locomotion and manipulation in different gravitational environments requires a robust form factor, with limbs capable of operating as both locomotive limbs and as manipulators, as needed. Thus, design considerations such as range of motion, actuation method, assembly, and control approach needed to be taken into account when designing the limb. For minimum functionality of the full limb over a range of motion that approximates that of a human arm, a 2 DOF shoulder/hip and 1 DOF elbow/knee were recommended, as this would allow for basic trajectories to be tested and this would allow for planning for packaging the actuation components. For clarity, the joints shall be referred to as the hip and knee joints for the rest of this paper. The simplified TGR limb is

Table 3.1: Variables

Variables	Meaning
k	Spring stiffness
d_{BENE}	Diameter of BENE
d_{hub}	Diameter of the central hub of the BENE
h_{slot}	Depth of the slots that hold the leaf springs
h_{ext}	Height of the extrusions
n_{sec}	Number of identical sections in the BENE
$n_{springs}$	Number of springs in BENE
$n_{springs\_sec}$	Number of springs in a section
L	Active length of the leaf spring
h	Leaf spring thickness
b	Leaf spring width
FOS_{des}	Desired Factor of Safety (FOS)
FOS	Calculated FOS
θ_k	Stiffness offset angle
θ_{max}	Maximum angular displacement
θ_{ext}	Angle inhabited by all extrusions in a section
θ_{needed}	Angle needed in a section for desired maximum bending/jamming
θ_{knee}	Measured angle of the knee
σ_y	Yield stress
σ_{max}	Maximal stress
E	Modulus of elasticity
I	Area moment of inertia
τ_{max}	Max use-case torque
τ_{spring}	Torque on a single leaf spring
τ_{BENE}	Torque on a single BENE module
τ_{limb}	Torque from lower limb weight
g	Gravitational acceleration
m	Mass of the body

shown on the TGR in Fig. 3.1.
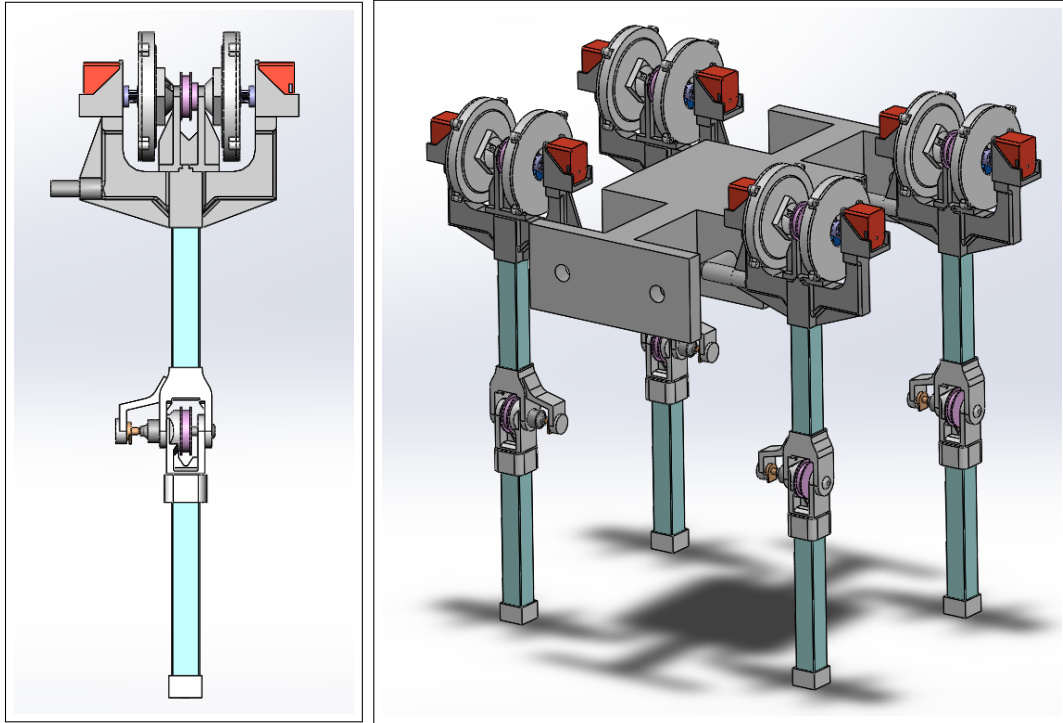
Figure 3.1: The TGR limb (left) mounted on the preliminary TGR (right). Preliminary TGR CAD model courtesy of TGR project teammate, Felix Sanchez.

3.1.2 Actuation Method

As the TGR is expected to be able to operate in Lunar and orbital environments, potentially within small, enclosed spaces (ISS or similar environments of operation), the actuation methods needed to be carefully considered. As the robot would share a space with humans, sensitive equipment, and a dynamic or unpredictable environment, passive joint compliance was deemed necessary, as this would allow the TGR to mitigate collisions and impacts. Moreover, compliant joints would allow for a more human-safe environment, as the robot would be able to safely interact with humans. Passive compliance is achievable through soft robotics and elastic elements. However, there is a trade-off in precision when using a compliant actuation method.

With increased compliance, there is a more pronounced loss in trajectory precision. However, this trade-off can be partially mitigated through variable stiffness actuation (VSA), as this actuation approach allows joint stiffness to be a controllable degree of freedom, thus allowing for stiffness compensation to trajectory errors. Due to the expected loading from walking trajectories and manipulation of the environment or objects of interest, it was determined that a series-elastic, antagonistic actuation method would provide ideal actuation method for the TGR.

As a VSA method, antagonistic actuation allows for decoupled position and stiffness control [12]. By controlling the preload on the springs, the equilibrium point between them can be used to independently and simultaneously modify the equilibrium position and equilibrium stiffness of the system. Thus, an antagonistic system would allow for variable stiffness, which could benefit the safety, efficiency, and effectiveness of operation [12]. For instance, a variable stiffness joint could be more compliant upon detecting a collision, and stiffened as needed when lifting heavy loads, thus reducing the operation torque of the motors, which allows for flexibility in operation between rigid motion and compliant motion. A use case for flexible operation using could be for walking efficiency, where the TGR could use the energy stored in the elastic element to help it push off the ground in a walking trajectory, as that energy is passively stored from the step-down and weight transfer motion. The knee joint would be more compliant upon foot touchdown, gradually stiffened as weight is transferred over the limb, and then actuated during the push-off motion using both the stored energy and the actuators.

3.1.3   Form Factor and Configuration

To minimize joint torques, thus increasing operation efficiency and reducing the magnitudes of torques involved in rotational dynamics (necessary for micro-gravity),

it was decided that actuators be mounted as close to the main body of the TGR as possible, with a remote actuation approach being implemented for the knee joint and future planned actuated joints or elements, such as the wrist and end effector. A gear belt pulley system was used to actuate the knee, with the elastic elements and motors being mounted on opposite sides of each other on the proximal pulley's axis, as shown in Fig. 3.2.
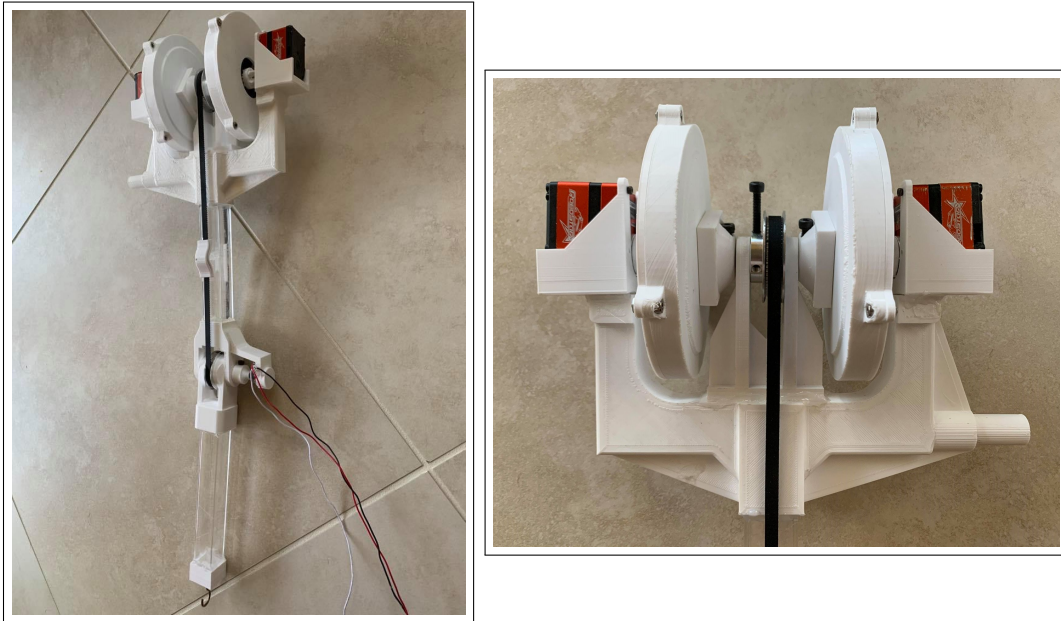
Figure 3.2: The TGR limb with its gear belt pulley actuation method for the knee joint (left) and the dual BENE assembly (right).

As the elastic elements would be operating in parallel, the equivalent stiffness of the knee joint can be described as:

$$k_{eq} = k_1 + k_2 \tag{3.1}$$

For the verification of the functionality of this actuation approach at the knee, the prototype limb was simplified so that the hip joint was reduced to a single unconstrained, rotational degree of freedom around the axis parallel to the knee's rotation

axis, as shown in Fig. 3.3. Thus, a "straight leg" and "bent leg" configuration could be achieved under a gravitational load by merely actuating the knee joint.
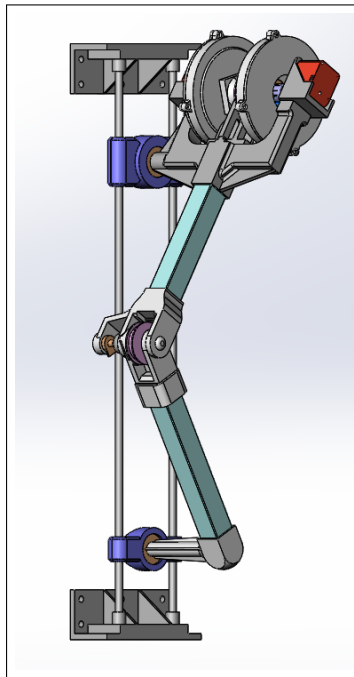
Figure 3.3: The TGR limb mounted onto test rails to enable controlled "free-fall". The indigo components are slide bearing mounts that allow the hip and foot to freely rotate.

3.2   Bidirectional Elastic Nonlinear Element (BENE)

3.2.1   Design and Development

As the system required variable stiffness antagonistic actuation, two nonlinear elastic elements would be needed, as described in [12]. By using nonlinear springs, the system becomes capable of varying joint position and joint stiffness, which would not be possible with linear springs, which have a constant stiffness. Thus, a compact, bidirectional, nonlinear element able to be used in a rotary joint was needed. For a

small form factor approach and due to packaging constraints, where it is expected that all actuation components will eventually be located within the limb, a torsional spring similar to that shown in Fig. 3.4 was required. This spring is described in [22], and a similar implementation can be found on R2 [23]. However, due to the cost of materials and fabrication of creating a similar custom torsional spring, a lower-cost, more customizable solution needed to be found.

Figure 3.4: A bidirectional torsional spring developed for use in SEA for knee assistance. The spring has a 85mm diameter and is made of VACO 180T (maraging steel 300), which puts the production cost at several hundred dollars [22].

The bidirectional nature of leaf springs made them ideal for implementation in the TGR system; however, uniform leaf springs have linear stiffness profiles. In order to create a nonlinear stiffness elastic element, the leaf springs were implemented in a spoke-like manner where they could collide with a geometric pattern of extrusions, as shown in Fig. 3.5.

For this implementation, a uniform leaf spring design was used in which all jamming elements (the springs) were identical in length, thickness, width, and material. 1095 blue spring steel was selected due to its strength and elasticity properties as

Figure 3.5: An open BENE module. The leaf springs are arranged like spokes from a central hub and jam with the geometric extrusions when bending.

well as its low cost. The material selection and size of the leaf spring determined the potential bending angle of the spring, as its yield strength and length were important factors in determining maximum bending angle. It is important to note that the customizability of the BENE module would allow for varying spring elements to be used, thereby greatly expanding the potential stiffness profiles it is capable of having. The equations used in the design of the BENE module are as follows:

From beam bending:

$$I = \frac{b * h^3}{3} \tag{3.2}$$

$$\theta_{max} = sin^{-1}\left(\frac{2L\sigma_y}{3Eh}\right) \tag{3.3}$$

$$\sigma_{max} = \frac{\tau_{BENE}}{In_{springs}} \tag{3.4}$$

Factor of safety:

$$FOS = \frac{\sigma_y}{\sigma_{max}} \tag{3.5}$$

Stiffness:

$$k = \frac{d\tau_k}{d\theta_k} \tag{3.6}$$

The design method for the BENE module is as follows:

Algorithm 1: BENE Configuration Function

Result: Generated Stiffness Profile
Begin

  Constants: d_{hub}, h_{slot}, h_{ext}, θ_{ext}, n_{sec};
  User Inputs: d_{BENE}, τ_{max}, FOS_{des}, $n_{springs\_sec}$, θ_{travel};
  After material selection: E, σ_y, h, b, k;
  (Note: multiple different springs can be used in the same design)
  Determine $L_s pring$;
  Use Eq. 3.2;
  Use Eq. 3.3;
  while $FOS < FOS_{des}$ **do**
    | Increment $n_{springs}$
    | Use Eq. 3.4;
    | Use Eq. 3.5;
  end
  Find angle at which bending begins for each spring;
  Find θ_{needed} based on previous step;
  Use Eq. 3.4 to find σ_{max} for configuration;
  Use Eq. 3.5 with new σ_{max} to find FOS_{BENE};
  if $theta_{needed} <= $ angle of a section **then**
    | **if** $FOS_{BENE} < FOS_{des}$ **then**
    | | This is a valid configuration.
    | **else**
    | | This is an invalid configuration;
    | **end**
  else
    | This is an invalid configuration
  end
  if valid configuration **then**
    | theta = 1:40 Use Eq. 3.6 to solve for τ_{spring}
    | Use Eq. 3.6 to solve for k-profile
  else

  end

By using this design algorithm, which was implemented into a MATLAB function, BENE module configurations can be created and validated before manufacturing begins. The approach is highly configurable and allows for the modification of parameters such as amount of springs that share a bending angle to the k-values and

materials of each individual jamming element (the leaf springs, in this implementation). For example, if maximum stiffness was desired such that compliance was negligible (for high precision tasks), an element could be integrated with a k-value equivalent to a rigid body. This would allow for variable stiffness from maximum compliance to near-total rigidity. A sample stiffness plot is shown in Fig. 3.6.
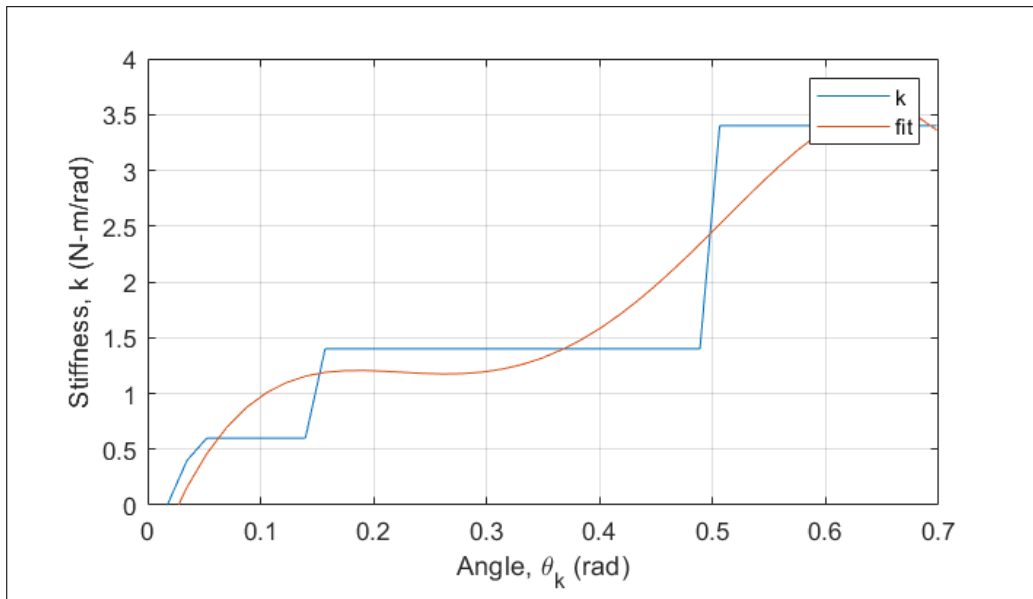

Figure 3.6: A sample stiffness profile plot from the BENE Configuration Function.

For the selected form factor, the maximum bending angle of a leaf spring was 40 degrees. Factor of safety evaluations, done in the algorithm, were used to determine the number of springs needed to operate under the expected joint torques. The length of the springs was limited by the required compact size and θ_{max}, and the geometric profile within the module was determined by the available internal circumference available as well as the desired stiffness profile.

With the BENE module created, it was placed in the configuration shown in Fig. 3.2 to be used in antagonistic actuation. As this system used bidirectional torsional springs, the model differs from that described in Fig. 2.5. A closer representation can be found in Fig. 3.7. From the first diagram, it is clear that the

BENE modules are rotated in the same direction, the lever rotates with them, as the equivalent equilibrium position is being directly rotated. As a result of the synchronous rotation, neither spring is loaded against the other, resulting in no stiffness change. From the second diagram, it can be gathered that when the BENE modules synchronously rotate opposite from each other, the stiffness will increase. From the third diagram, a similar conclusion can be drawn but with decreasing stiffness. The second and third diagrams do not involve a change in the equilibrium position, only a change in the angle offset between the springs (θ_k). Therefore, it is possible to adjust stiffness and position independently. However, by combining the change in equilibrium position between the springs as well as the θ_k, it is possible to control both simultaneously.
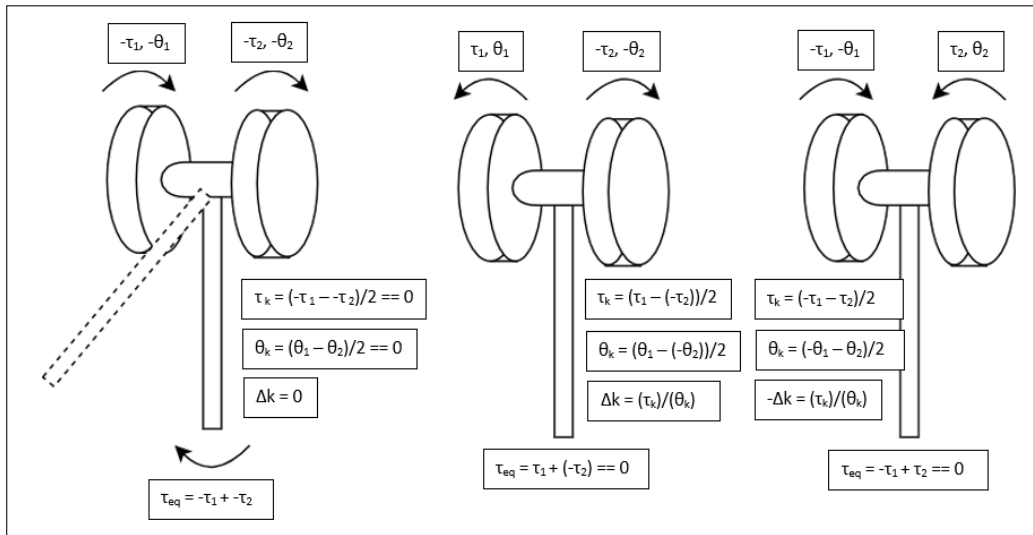

Figure 3.7: An open BENE module. The leaf springs are arranged like spokes from a central hub and jam with the geometric extrusions when bending.

3.2.2 Prototype Specification

In Fig. 3.5 it is clear that the geometric profile extrusions have straight profiles rather than curved or irregular profiles—this is primarily due to the limited available

space for rotation, as curved profiles would take up more of the internal circumference.

The stiffness profile was determined experimentally by loading the module through a range of angular displacements (recorded with a potentiometer) and recording the change in torque (using a strain gauge). These valus were then used with Eq. 3.6 to determine the stiffness values. The resulting stiffness profile, shown in Fig. 3.8, represents the average of 6 trials and is shown in the following equation:

$$k = 13.938\theta_k{}^3 - 14.614\theta_k{}^2 + 5.1518\theta_k + 0.0153 \tag{3.7}$$
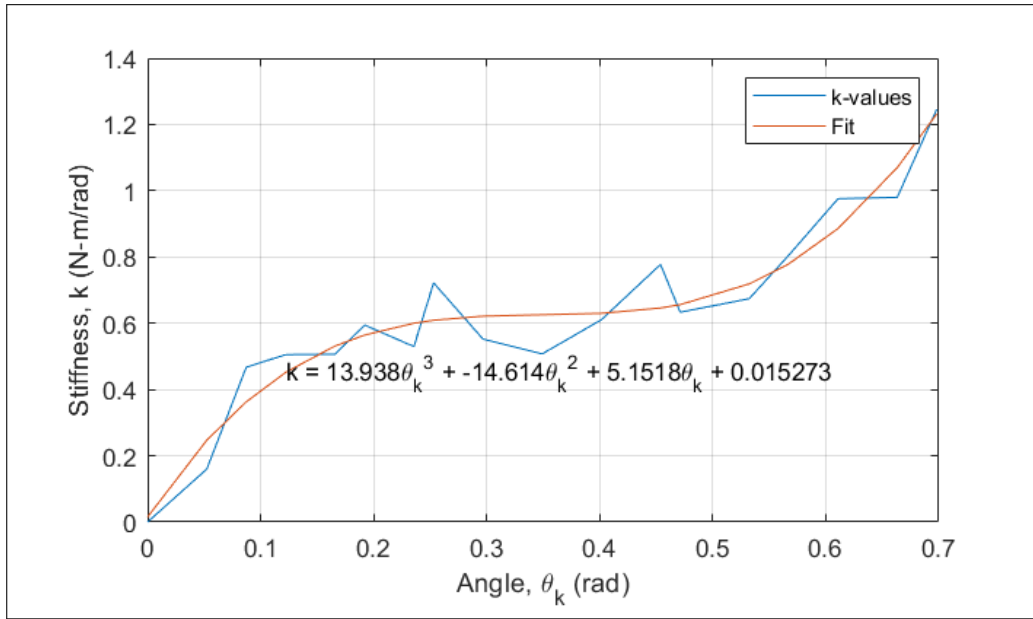
Figure 3.8: The experimentally derived BENE stiffness profile.

While sensor noise, friction, and calibration errors did cause some inconsistencies, the general trend equation, as shown in the figure, follows the expected behavior of the desired nonlinear spring profile.

The BENE module is scale-able to different load scenarios by varying the spring material, spring length, and internal geometric profile. A single module costs an

25

estimated \$5.50 to produce given the 1095 spring steel material selection, which is low compared to the cost to produce a custom nonlinear torsion spring disc similar to that described in [22]. As a bidirectional, nonlinear, elastic element, the BENE is a low-cost solution that could have many bio-mimetic robotic research applications due to its low production cost.

Chapter 4

Experiments

4.1 Drop Test

To verify the functionality of the BENE module as the elastic element in an antagonistically actuated system, the collision and impact mitigation capabilities were evaluated. For this experiment, the TGR limb was set to a designated starting angle off of the straight leg position (zero degree, or home, position), and then dropped in simulated Lunar gravitational conditions. The gravitational acceleration of the Moon was approximated by mounting the limb onto rails fixed at 16 degrees from the horizontal. By assembling the test bed in such a manner, the component of the gravitational force that is parallel to the rails approximates the effects of Lunar gravitational acceleration, to which allows the limb to experience simulated Lunar free fall. This test setup is shown in Fig. 4.1. For this experiment, the foot and hip were aligned along the vertical axis and the foot was allowed to freely rotate on an axis parallel to the hip, simulating ankle rotation. With simulated hip and ankle rotation, the impacts could be absorbed better at the knee, as this provided a more natural motion.
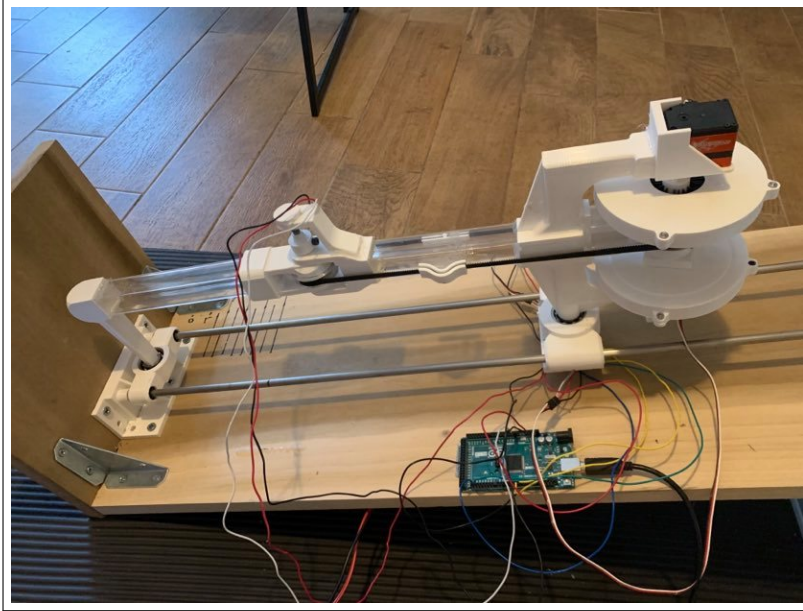
Figure 4.1: The drop test experiment test setup. The rails are set to a 16 degree angle from the horizontal in order to simulate Lunar gravity conditions and the TGR limb is dropped from a height of 5.08 cm.

The linear acceleration (along the axis of the rails) was measured with an inertial measurement unit (IMU), and validated as approximating the gravitational acceleration of on the Moon, which is 1.62 m/s^2. From the resulting IMU and knee angle data (measured with a potentiometer), the impact mitigation capability of the module could be observed. The limb was dropped from a height of 2 in. (5.08 cm), as this height allowed for substantial enough impact forces to clearly show the impact behavior of the system without plastically deforming the leaf springs in the BENE module. The drop test was conducted at 4 stiffness offset angles (θ_k): 0, 10, 20, and 30 degrees. These offset angles were tested at 4 knee angles (θ_{knee}): 15, 30, 45, and 60.

4.2 Controlled Stiffness

As an antagonistically actuated system, the stiffness and position are decoupled and can be controlled independently. In order to show the capability of the system for this compliant actuation method, an unknown load within the range of 0.070kg-0.170kg was placed at the end of the limb and then lifted in 10 degree steps. The experimental setup, shown in Fig. 4.2, consisted of constraining the hip DOF so that only the knee angle could vary and using an end effector that could carry a load.

Figure 4.2: The control test experiment setup, which features the load-lifting end effector and the load reservoir. Here the hip is constrained by the additional brackets mounted behind the hip joint.

The control loop compares the desired knee angle to the measured knee angle (from the potentiometer) and uses the error to determine the current equilibrium

angle of the BENE module. In this case, the equilibrium angle is the angle at which the BENE is able to reach equilibrium while loaded. Using this angle, the current stiffness (k) is determined by plugging that angle value into Eq. 3.7. This is then used to determine the current measured torque at the BENE module:

$$\tau_{BENE} = k * \theta_k \tag{4.1}$$

This torque and the current measured knee position are then used to derive the estimated mass (under Earth gravitational conditions) of the load:

$$m = \frac{\tau_{BENE} - \tau_{limb}}{gr(sin(\theta_{knee}))} \tag{4.2}$$

Then, given the desired knee position, θ_d, and the estimated load, the estimated load torque at the end of the next step can be calculated using the following equation:

$$\tau_{next} = mgr(sin(\theta_d)) + \tau_{limb} \tag{4.3}$$

This predicted torque value is then compared to the torque values for each θ_k, which can be found by plugging the θ_k values into Eq. 3.7, which will reveal the θ_k needed for the next step, thus allowing the system to stiffen as needed. The ability of the system to predictably vary stiffness with position was evaluated in this experiment. The variable stiffness controller was first evaluated with a 0.070kg mass, a 0.100 kg mass, and 0.130kg mass. The controller was then tested in a "varying load" scenario, where the mass was increased from 0.080kg to 0.125kg and then to 0.170kg during the trajectory, with a 0.045kg mass being added at every 30 degrees.

4.3 Collision Response

Collision detection is required for the safe operation of a system that operates either within a dynamic environment or in a shared space with humans or sensitive equipment. With its antagonistic actuation method, the TGR limb could detect and mitigate collisions. For this experiment, the same setup is used as in Fig. 4.2, with the exception of introducing an obstruction to the trajectory, as shown in Fig. 4.3. The limb is operated similar to how it is in the controlled stiffness experiment; however, it actively checks for collisions.
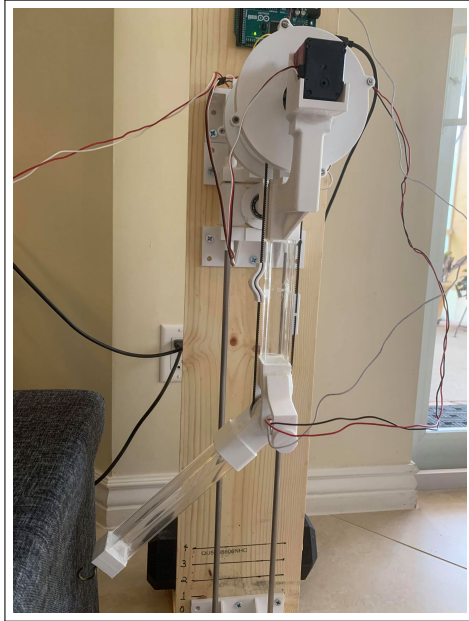

Figure 4.3: The collision response test setup without a mounted load.

As an addendum to the controlled stiffness algorithm, when the controller detects that error exceeds the collision threshold, it will "slow down" the trajectory by taking a smaller step and reducing the stiffness to allow for a more compliant collision. If by the end of that step the error still exceeds the threshold, the limb will return to its zero position.

Chapter 5

Results

5.1   Drop Test

The drop test was used to verify the collision and impact mitigation ability of the TGR limb with the BENE modules used in antagonistic actuation. The acceleration data was measured with an IMU mounted at the freely rotating hip, and the position data was measured with a potentiometer mounted at the knee. From the results shown in Fig. 5.1-5.4, it is clear that as stiffness increases, the compliance decreases. Plots (a)-(d) show the acceleration data, which depicts increased oscillations as θ_{real} increases and decreases. Plot (e) shows the filtered θ_{real} data, which supports the aforementioned conclusion from the acceleration data.

5.2   Controlled Stiffness

The controlled stiffness test was used to verify the variable stiffness capabilities of the BENE modules in an antagonistic actuation configuration. The potentiometer at the knee was used to measure the knee position, as in the drop test experiment. From the results shown in Fig. 5.5-5.7, it is clear that the limb was able to follow the
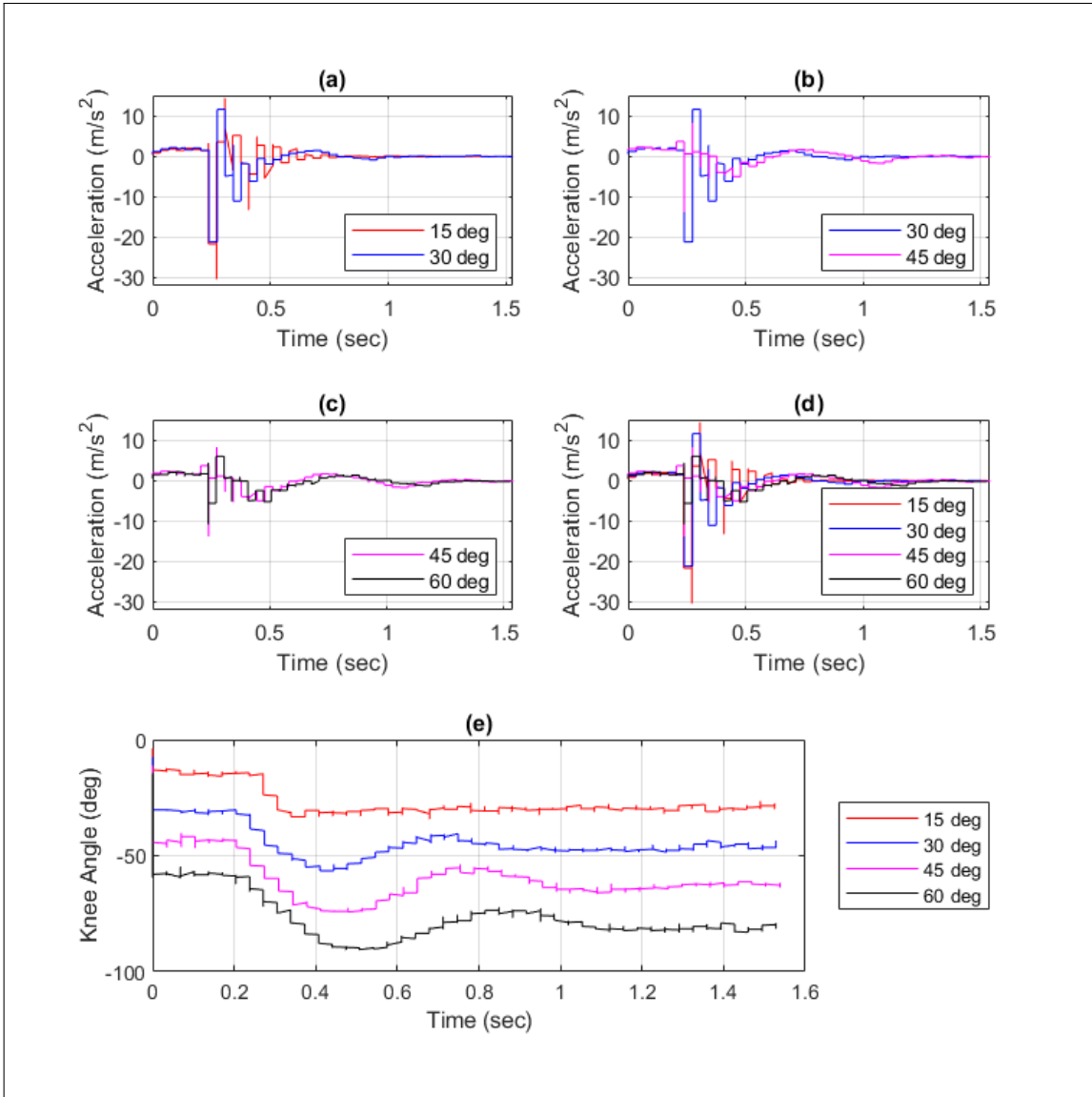
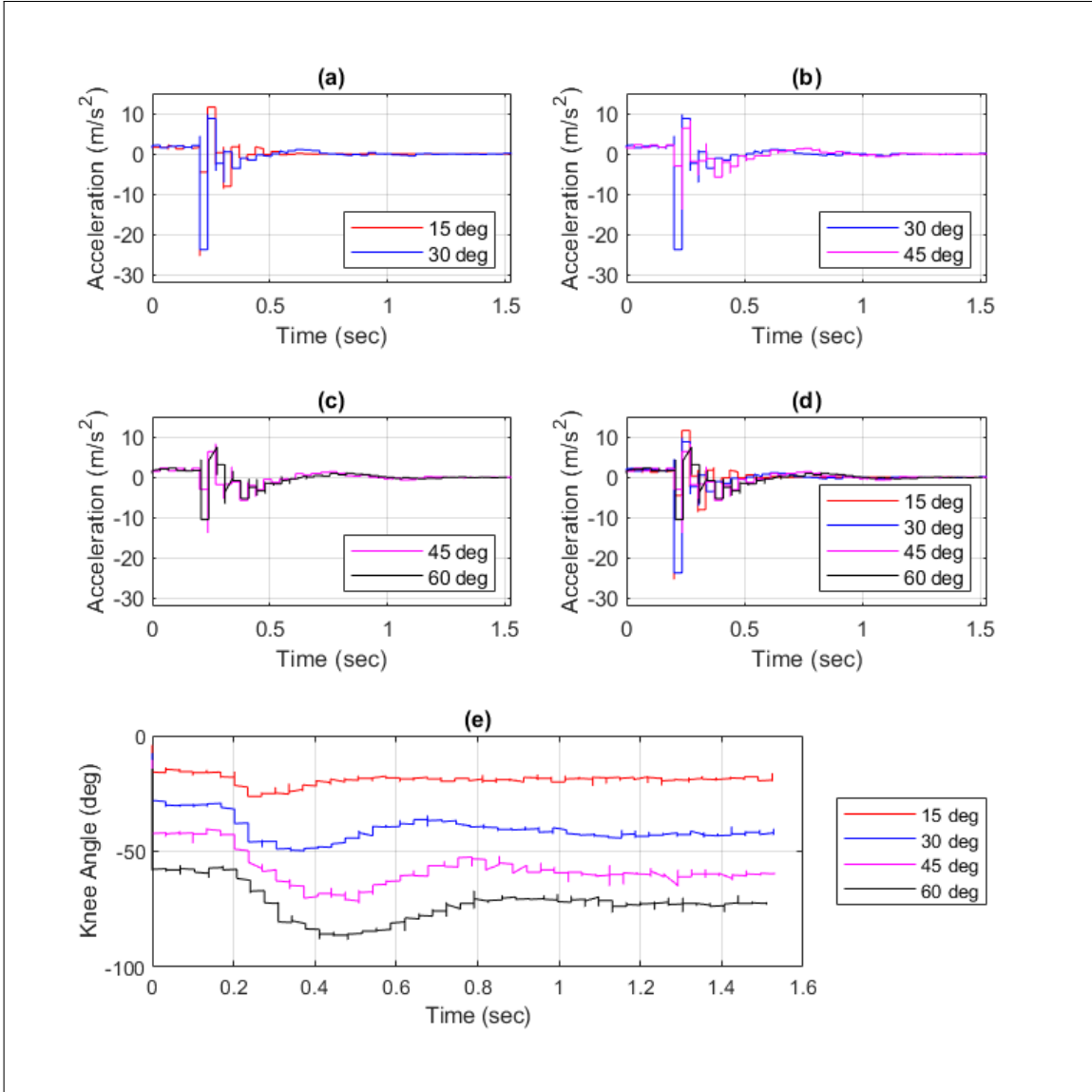Figure 5.1: Drop test results at $\theta_k = 0$

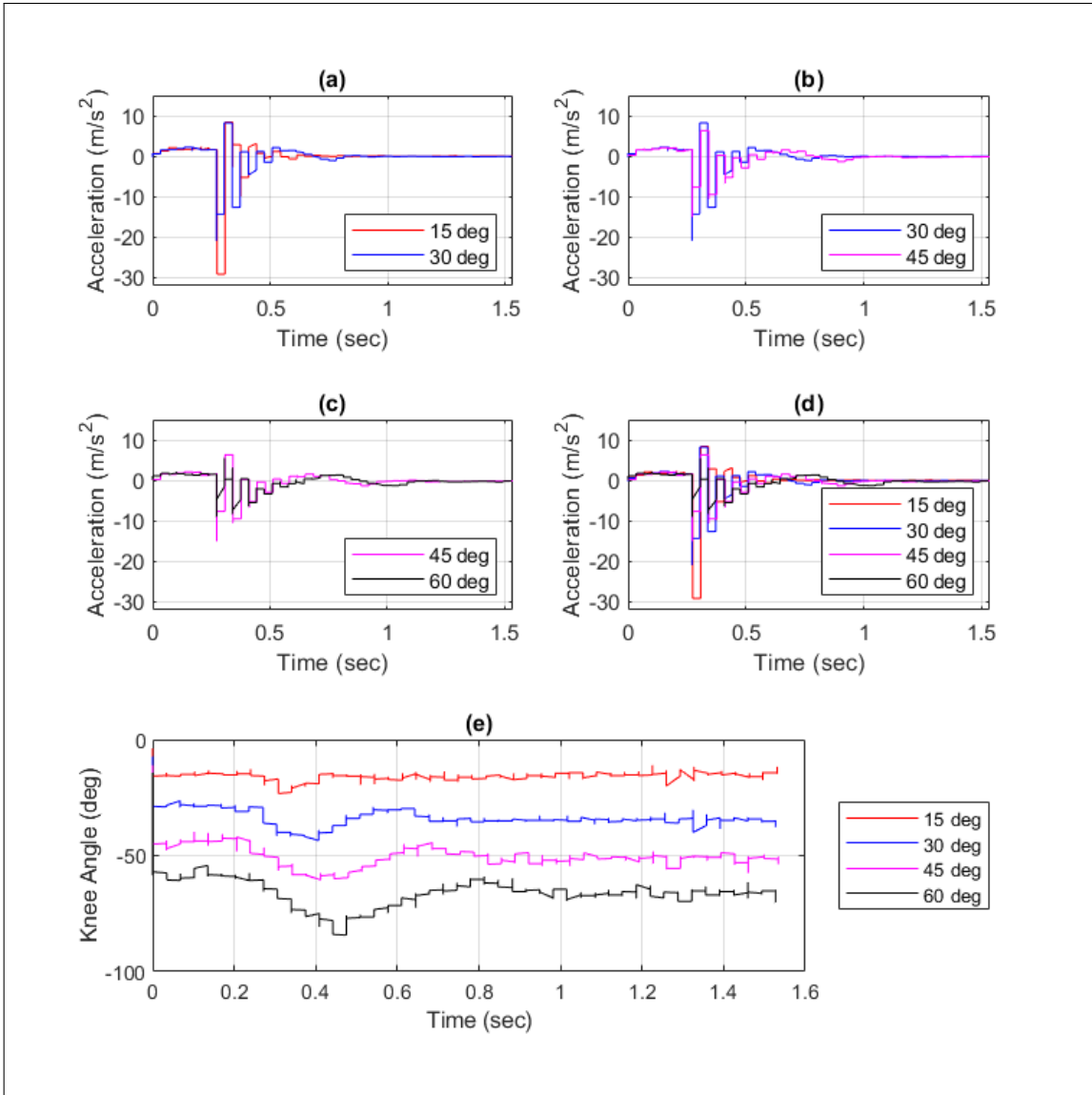Figure 5.2: Drop test results at $\theta_k = 10$

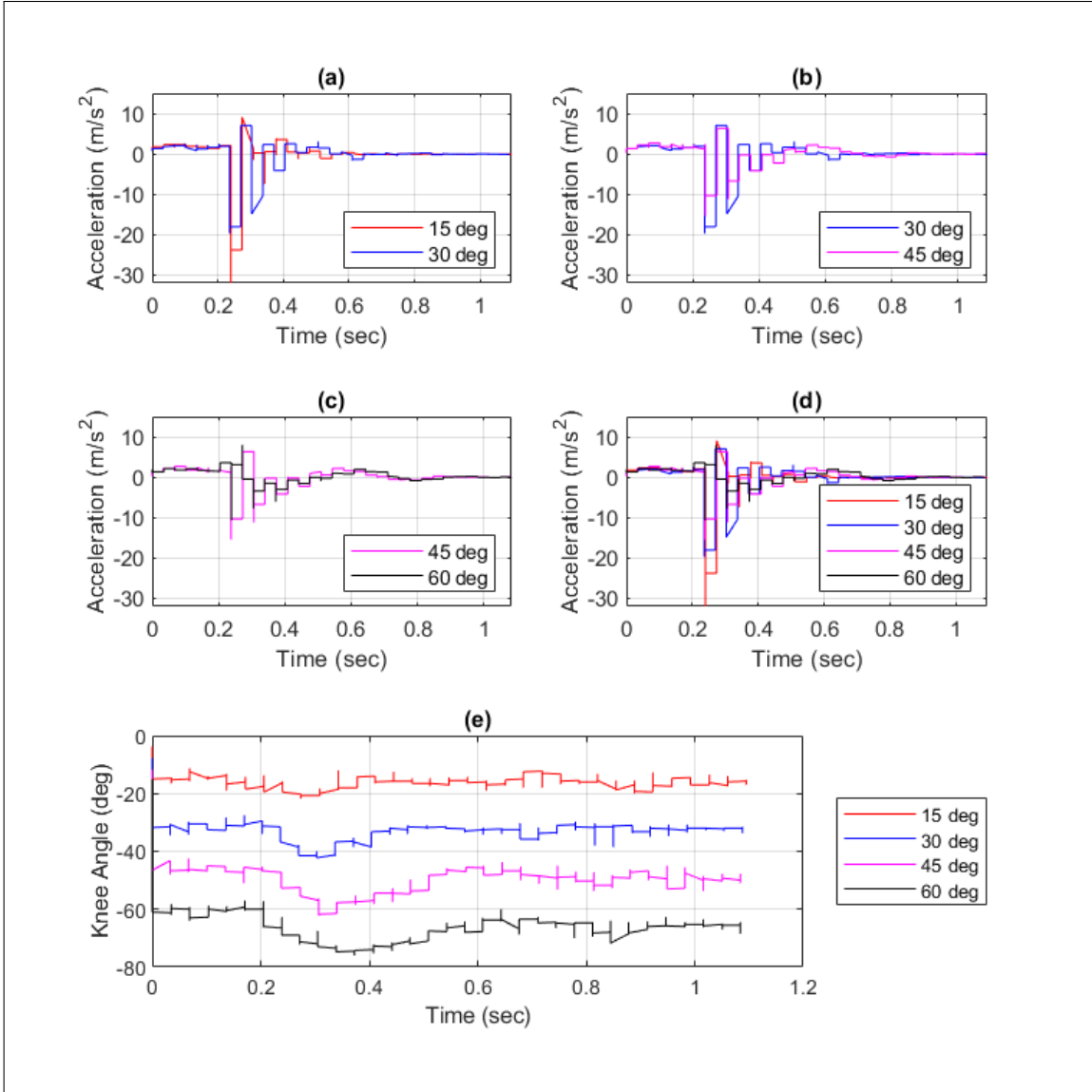Figure 5.3: Drop test results at $\theta_k = 20$

Figure 5.4: Drop test results at $\theta_k = 30$

desired trajectory while carrying a load. The results present two scenarios, controlled and uncontrolled, and the controlled trajectory has much lower deviation from the desired trajectory than the uncontrolled trajectory, where larger load caused a larger error due to the bending of the non-preloaded springs. The torque plots show how the controller is able to predict the needed torque and use it to follow the desired trajectory. The estimated mass plots depict how the controller is able to estimate and converge to the correct mass of the load by the end of the trajectory. Fig. 5.8 shows how the higher loads required higher spring stiffness values.
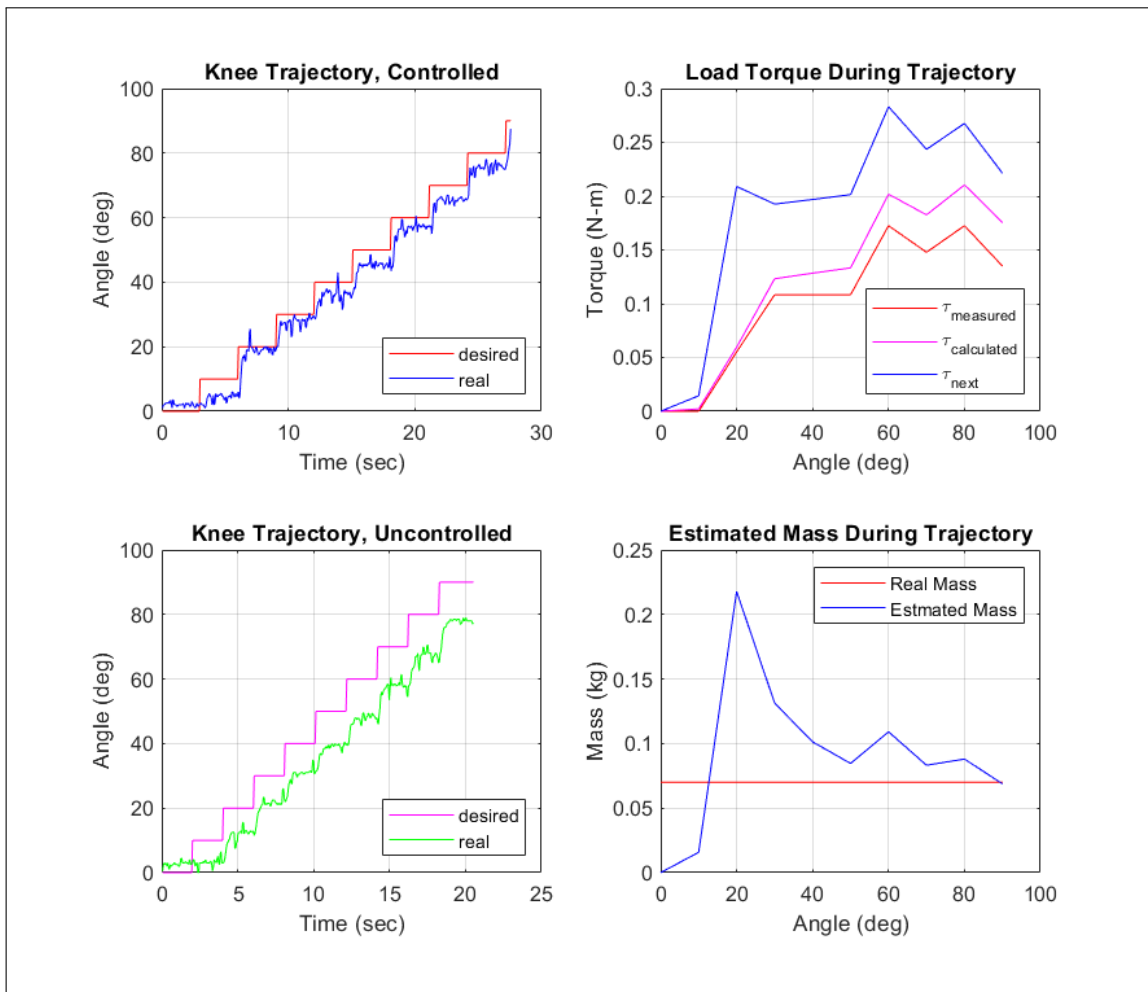

Figure 5.5: Control test results with a 0.070kg load

The varying load trial, the results of which are shown in Fig. 5.9, provided
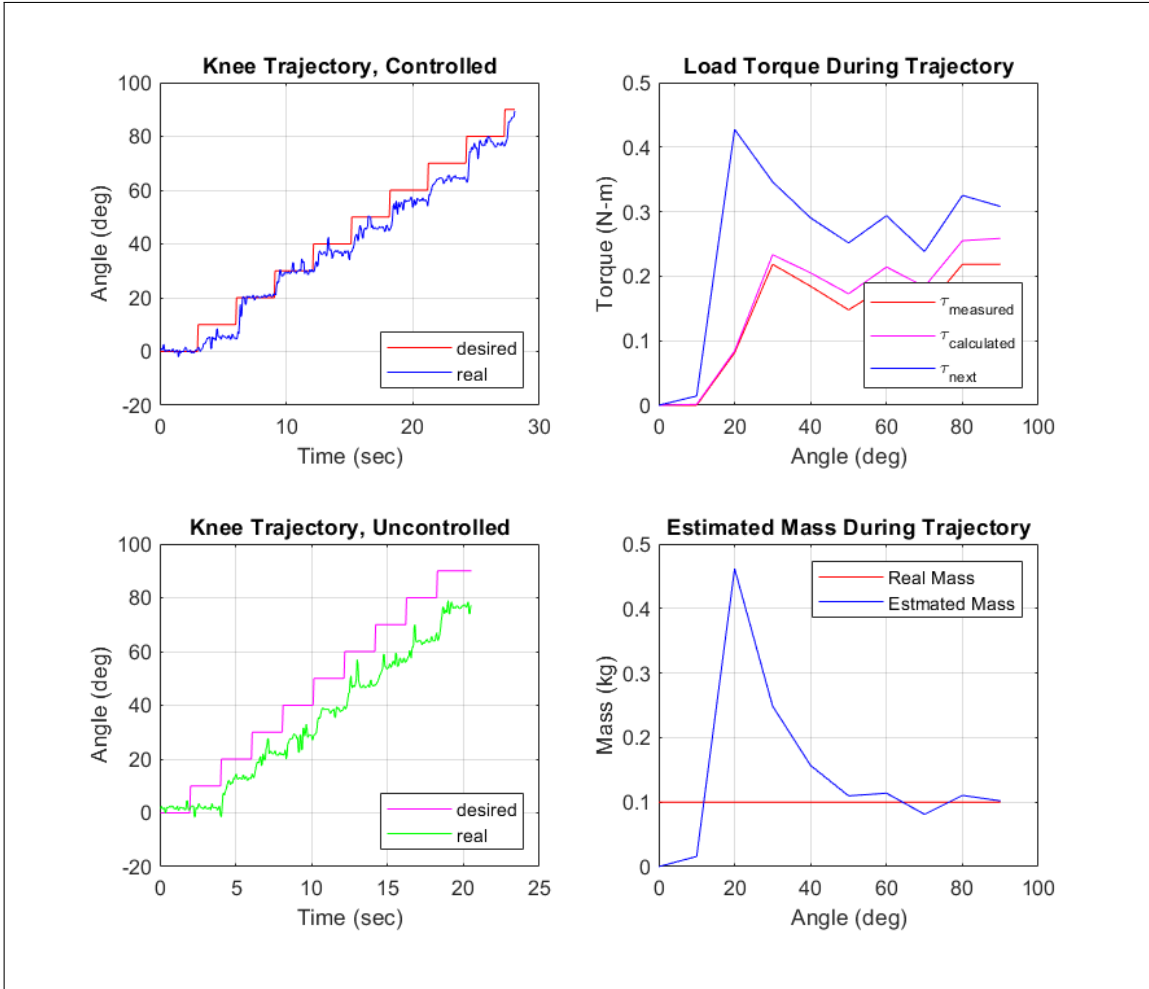
Figure 5.6: Control test results with a 0.100kg load
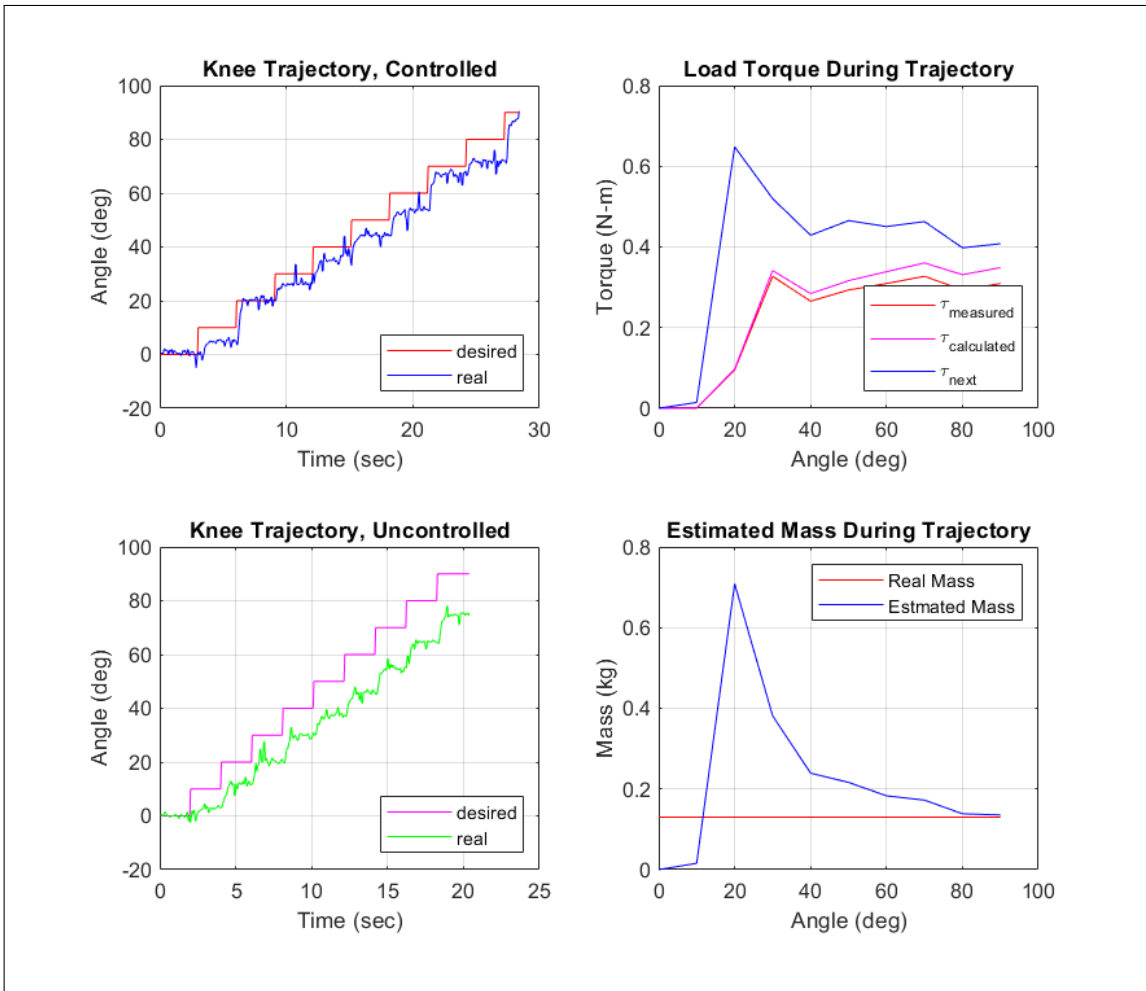
Figure 5.7: Control test results with a 0.130kg load
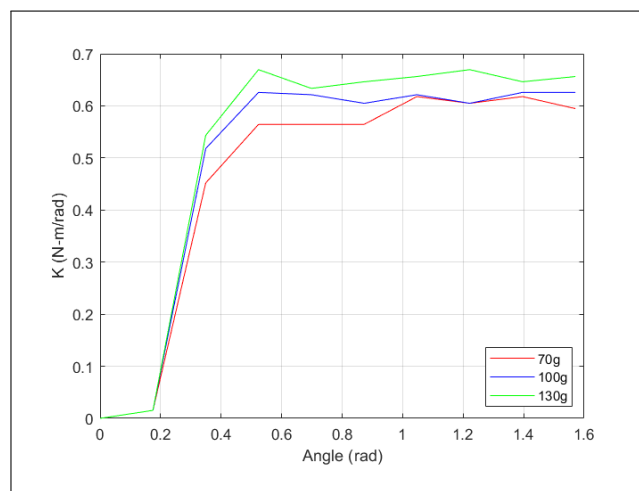
Figure 5.8: Comparison of K-values in the trajectory for each load

results that show the efficacy of the BENE module in an antagonistically actuated system. The limb was able to closely follow the desired trajectory even as the load is varied, the predicted torques were close to the measured and calculated torques, and the estimated mass was able to converge towards the actual final load. Moreover, according to Table 5.1, which shows the percent error between the real trajectories and the desired trajectories, there is a near 50% error reduction when using the controller.
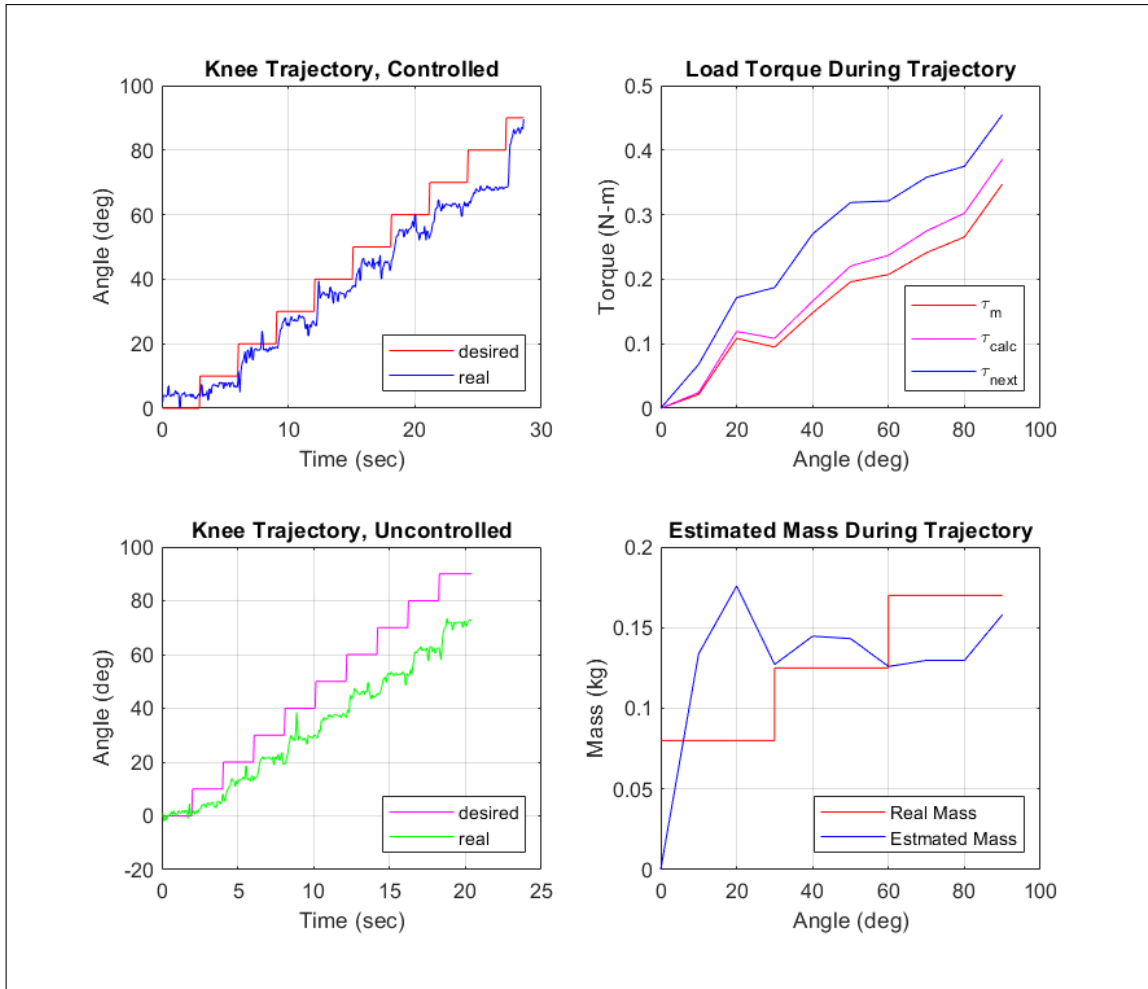
Figure 5.9: Control test results with a varying load (from 0.080kg to 0.125kg to 0.170kg)

From Table 5.2, is is clear that the controller was able to have the estimated

Table 5.1: Percent Error in Trajectories For Controlled Stiffness Experiment

Control Approach	0.070kg	0.100kg	0.130kg	Varying	Average
Controlled	15.97	14.42	17.62	15.56	15.89
Uncontrolled	29.35	32.77	33.75	32.07	31.99

Table 5.2: Percent Error of Final Mass For Controlled Stiffness Experiment

| Real Mass (kg)	0.070	0.100	0.130	Varying	Average
Estimated Mass (kg)	0.0688	0.1019	0.1355	0.1580	31.99
Percent Error	1.71	1.90	4.23	7.06	3.73

mass converge to the real mass within an average percent error of 3.73. The largest percent error comes from the varying load trial, which is expected as the mass increases twice during the trajectory, forcing the controller to compensate.

5.3 Collision Response

The collision response test served to showcase the collision mitigation capability of the BENE module in a variable stiffness system. This experiment used the same setup as the controlled stiffness test. With a load placed at the end of the limb, the limb would follow its step-wise trajectory to 90 deg; however, an obstacle was introduced to prevent the limb from continuing its trajectory. The collision is detected just after the 15 second mark, and from the knee trajectory plot in Fig 5.10, it is clear that the control loop took a half step once error exceeded the collision error threshold. Stiffness was also immediately reduced so as to mitigate the collision. It is also clear that the system estimated a higher load as a result of the collision with the obstacle, as the load torque suddenly increased. The limb then returned to the home position.
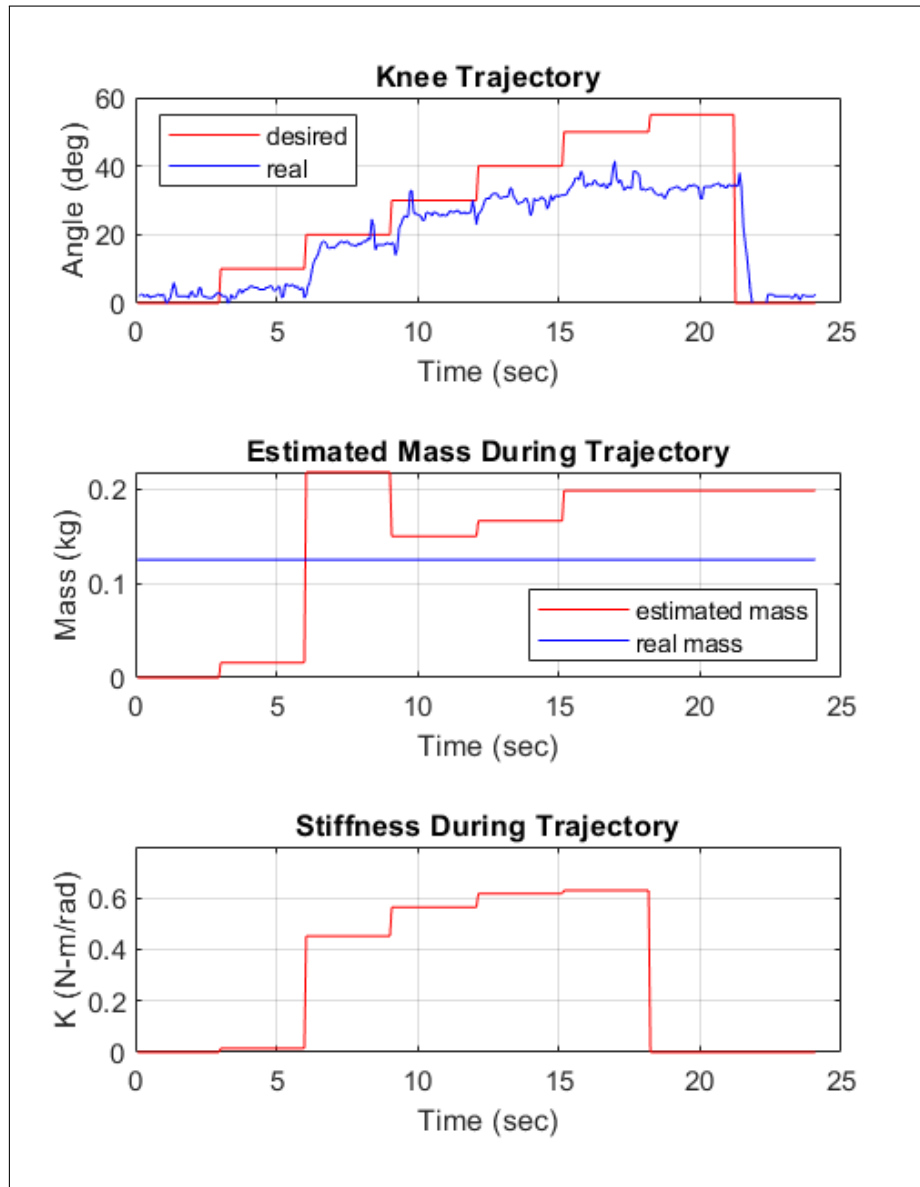
Figure 5.10: Collision test results with a load of 0.125kg

Chapter 6

Discussion

6.1   Drop Test

The drop test was able to successfully showcase the impact mitigation ability of the BENE-module-driven antagonistic actuation system. From the drop test data, it was clear that with increased compliance, the limb's ability to absorb impacts improved, as the initial impact deceleration the body experienced decreased and the body had a longer oscillation period. With varying BENE module configurations, such as using longer springs or different geometries, a softer impact could be achieved.

While the data trends were favorable, there were still errors and discrepancies in the data from the drop test. The noise from the potentiometer at the knee caused the values to occasionally drift beyond a difference of 5 degrees, which would cause inconsistencies. Moreover, as a result of manually dropping the limb from 2 inches, it is possible that there were small inconsistencies in the drop height. Having a better angular position sensor, such as an encoder or other similar rotary position sensor and an automated, actuated drop platform would reduce inherent errors as well as those caused by the experimental procedure.

For this experiment, the hip was free to rotate and the foot was attached to a bearing mounted on the slide rails in order to keep it aligned with the hip, which constrained the limb and allowed for free rotation of the foot. Future endeavors could expand on this experimental result by using an actuated hip and ankle, which would could improve the dampening of impacts and collisions.

6.2   Controlled Stiffness

The controlled stiffness test successfully demonstrated the variable stiffness capabilities of the BENE module in an antagonistically actuated system, thereby proving the viability of this actuation approach for the TGR limb. From Table 5.1, it was clear that the limb was able to follow the desired trajectory with a near 50% error reduction when using the controlled stiffness controller as opposed to using no controller. However, there was still an average 15.89% difference between the real and desired trajectories when using this controller. This discrepancy could be attributed to errors in the servo motor calibration, limb oscillations from stopping and starting each step, sensor noise from the potentiometer, and hysteresis caused by the compliance in the system. The servo motors, which were calibrated within a specific range of motion and were addressed directly with microsecond pulses (to reduce assumptions and error), differed slightly through their range of motion, which could cause discrepancies when applying θ_k to a step. The use of motors with real-time position feedback would allow for real-time tracking and adjustment of the motors, thereby increasing the accuracy of the controller.

Having a real-time controller would also reduce the effect of the magnitude of the initial mass estimate, which was likely caused by potentiometer noise and the 5 degree dead-band at zero position. This dead band is caused by tolerance errors

as well as the unloaded, un-stiffened springs, and can be avoided in future iterations by using a more precise manufacturing process. Furthermore, the BENE modules themselves could have slightly different profiles, as the spring profile used was experimentally derived and closely described the motion of both modules used. Manufacturing inconsistencies and tolerance issues could have affected spring performance, which would have affected how well the spring profile described the BENE modules.

In spite of these inconsistencies, the controlled stiffness approach was able to reliably converge on the correct mass, as shown in Table 5.2. With real-time control and better sensing, these results would likely be more accurate and more consistently reproduce-able.

6.3   Collision Response

The collision response test successfully demonstrated the basic collision detection protocol, in which the limb collides with an obstacle, reduces stiffness, and then returns to zero-position. It is clear how the estimated load increases and, in response, the necessary stiffness slightly increases. Because the error does not decrease, showing that the obstacle is still there, the half step is taken at around 18 seconds and stiffness is minimized in order to prevent further force exertion on the obstacle. The limb then returns to zero position, as shown at around the 22 second mark. This experiment had the same sources of potential error as the controlled stiffness test, and would benefit from real-time control in similar ways. However, real-time control would also allow for a more responsive and robust collision response procedure.

Chapter 7

Conclusion and Future Work

The simplified TGR limb, when paired with the novel BENE module, was able to showcase the potential of a future tetrapodal system utilizing antagonistic elastic actuation. The limb was able to mitigate impacts, as proved in the drop test, complete angular trajectories, as proved in the controlled stiffness test, and detect collisions, as proved in the collision response test. While only being a simple prototype, the capabilities displayed are expandable to full body obstacle collisions or impacts in locomotive trajectories, manipulator trajectories once the limbs have more DOF, and a more robust collision response procedure for manipulator trajectories. With the continued development of the TGR limb, which would involve refining the actuators, increasing the DOF, and creating a dedicated end effector capable of being used as a gripper and a foot, a prototype TGR could be created to showcase the capabilities of such a robot in both task oriented locomotion and manipulation.

Moreover, a design approach for the BENE module was developed that would allow future variable stiffness research to potentially incorporate varying BENE configurations with different stiffness profiles. The BENE module showed its capability for variable stiffness operation, thereby expanding the options of researchers looking

into compliant actuation. The module is not only lightweight, scale-able, and easily customized, but it is also easily accessible to research labs, in both necessary materials and required tools. Due to the ease of manufacturing, it is also an excellent option for the rapid prototyping and validation of compliant systems. The BENE module could have numerous applications across diverse fields that require compliant or variable stiffness actuation, such as space robotics, biomedical systems (such as prosthetic or rehabilitative devices), and collaborative robotics.

Bibliography

[1] Safe on Mars. National Academies Press, 2002.

[2] "Mars", NASA Solar System Exploration. [Online]. Available: https://solarsystem.nasa.gov/planets/mars/overview/.

[3] "Curiosity – NASA's Mars Exploration Program", NASA's Mars Exploration Program. [Online]. Available: https://mars.nasa.gov/msl/home/.

[4] P. Tompkins, A. Stentz, and D. Wettergreen, "Global path planning for mars rover exploration," presented at the 2004 IEEE Aerospace Conference Proceedings (IEEE Cat. No.04TH8720), doi: 10.1109/aero.2004.1367681.

[5] V. Dimitrov and T. Padır, "Human-in-the-loop control through kinematic redundancy resolution for space exploration rovers," 2016 IEEE Aerospace Conference, Big Sky, MT, 2016, pp. 1-7, doi: 10.1109/AERO.2016.7500936.

[6] "Mars Helicopter", Mars.nasa.gov, 2020. [Online]. Available: https://mars.nasa.gov/technology/helicopter/.

[7] Bualat M, Barlow J, Fong T, et al. Astrobee: developing a free-flying robot for the international space station. In: AIAA SPACE 2015 Conference and Exposition, Pasadena, California, 31 August–September 2015, Vol. 4643, pp. 1–10. American Institute of Aeronautics and Astronautics.

[8] Lee, D., Coltin, B., Morse, T., Park, I., Flückiger, L. and Smith, T. (2018). Handrail detection and pose estimation for a free-flying robot. International Journal of Advanced Robotic Systems, 15(1), p.172988141775369.

[9] "Robonaut2", Robonaut.jsc.nasa.gov. [Online]. Available: https://robonaut.jsc.nasa.gov/R2/pages/iss-mission.html.

[10] W. Wang, R. N. K. Loh, and E. Y. Gu, "Passive compliance versus active compliance in robot-based automated assembly systems," Industrial Robot, vol. 25, no. 1, pp. 48–57, Feb. 1998, doi: 10.1108/01439919810196964.

[11] G. A. Pratt and M. M. Williamson, "Series elastic actuators," presented at the 1995 IEEE/RSJ International Conference on Intelligent Robots

and Systems. Human Robot Interaction and Cooperative Robots, doi: 10.1109/iros.1995.525827.

[12] Ham, R., Sugar, T., Vanderborght, B., Hollander, K. and Lefeber, D. (2009). Compliant actuator designs. IEEE Robotics —& Automation Magazine, 16(3), pp.81-94.

[13] "JPL Robotics: System: The ATHLETE Rover", Www-robotics.jpl.nasa.gov. [Online]. Available: https://www-robotics.jpl.nasa.gov/systems/system.cfm?System=11.

[14] P. Hebert et al., "Mobile Manipulation and Mobility as Manipulation-Design and Algorithms of RoboSimian," J. Field Robotics, vol. 32, no. 2, pp. 255–274, Feb. 2015, doi: 10.1002/rob.21566.

[15] M. A. Diftler et al., "Robonaut 2 - The first humanoid robot in space," presented at the IEEE International Conference on Robotics and Automation, May 2011, doi: 10.1109/icra.2011.5979830.

[16] M. L. Latash, "Muscle coactivation: definitions, mechanisms, and functions," Journal of Neurophysiology, vol. 120, no. 1, pp. 88–104, Jul. 2018, doi: 10.1152/jn.00084.2018.

[17] Gaylord, RH (1958) Fluid actuated motor system and stroking device. Patent 2-238-058, USA, July 22.

[18] M. Meller, J. Chipka, A. Volkov, M. Bryant, and E. Garcia, "Improving actuation efficiency through variable recruitment hydraulic McKibben muscles: modeling, orderly recruitment control, and experiments," Bioinspir. Biomim., vol. 11, no. 6, p. 065004, Nov. 2016, doi: 10.1088/1748-3190/11/6/065004.

[19] Saivimal Sridar, Corey J Majeika, Phillip Schaffer, Matthew Bowers, Seiichiro Ueda, Andrew J Barth, Jon L Sorrells, Jon T Wu, Thane R Hunt, and Marko Popovic (2016) "Hydro Muscle - a novel soft fluidic actuator," 2016 IEEE International Conference on Robotics and Automation (ICRA), pp 4014-4021

[20] Matthew Bowers, Chinmay Harmalkar, Ankur Agrawal, Abhishek Kashyap, Jonathan Tai, and Marko Popovic (2017) "Design and test of biologically inspired multi-fiber Hydro Muscle actuated ankle," Proceedings of 2017 IEEE International Workshop on Advanced Robotics and its Social Impacts, March 8-10, 2017, University of Texas at Austin, Austin, TX, USA

[21] F. Petit, M. Chalon, W. Friedl, M. Grebenstein, A. Albu-Schaffer, and G. Hirzinger, "Bidirectional antagonistic variable stiffness actuation: Analysis, design —& Implementation," presented at the 2010 IEEE International Conference on Robotics and Automation (ICRA 2010), May 2010, doi: 10.1109/robot.2010.5509267.

[22] F. Sergi, D. Accoto, G. Carpino, N. L. Tagliamonte, and E. Guglielmelli, "Design and characterization of a compact rotary Series Elastic Actuator for knee assistance during overground walking," presented at the 2012 4th IEEE RAS —& EMBS International Conference on Biomedical Robotics and Biomechatronics (BioRob 2012), Jun. 2012, doi: 10.1109/biorob.2012.6290271.

[23] M. A. Diftler et al., "Robonaut 2 - The first humanoid robot in space," presented at the IEEE International Conference on Robotics and Automation, May 2011, doi: 10.1109/icra.2011.5979830.

[24] C. Listenbee, "Kavraki Lab develops framework for NASA's Robonaut 2", Rice Computer Science. [Online]. Available: https://csweb.rice.edu/robonaut2.

Appendix A

Contact

Please email the author at (jflorezcastillo AT wpi DOT edu) for GitHub access to the project repository.